Bio-Design and Manufacturing (2024) 7:14–30
https://doi.org/10.1007/s42242-023-00246-2

RESEARCH ARTICLE

Microarrow sensor array with enhanced skin adhesion for transdermal continuous monitoring of glucose and reactive oxygen species

Xinshuo Huang[1] · Baoming Liang[1] · Shantao Zheng[1] · Feifei Wu[1,3] · Mengyi He[1] · Shuang Huang[1] · Jingbo Yang[2] · Qiangqiang Ouyang[4] · Fanmao Liu[4] · Jing Liu[4] · Hui-jiuan Chen[1] · Xi Xie[1,2]

Received: 31 January 2023 / Accepted: 13 May 2023 / Published online: 2 September 2023

Abstract

Conventional blood sampling for glucose detection is prone to cause pain and fails to continuously record glucose fluctuations in vivo. Continuous glucose monitoring based on implantable electrodes could induce pain and potential tissue inflammation, and the presence of reactive oxygen species (ROS) due to inflammation may affect glucose detection. Microneedle technology is less invasive, yet microneedle adhesion with skin tissue is limited. In this work, we developed a microarrow sensor array (MASA), which provided enhanced skin surface adhesion and enabled simultaneous detection of glucose and H_2O_2 (representative of ROS) in interstitial fluid in vivo. The microarrows fabricated via laser micromachining were modified with functional coating and integrated into a patch of a three-dimensional (3D) microneedle array. Due to the arrow tip mechanically interlocking with the tissue, the microarrow array could better adhere to the skin surface after penetration into skin. The MASA was demonstrated to provide continuous in vivo monitoring of glucose and H_2O_2 concentrations, with the detection of H_2O_2 providing a valuable reference for assessing the inflammation state. Finally, the MASA was integrated into a monitoring system using custom circuitry. This work provides a promising tool for the stable and reliable monitoring of blood glucose in diabetic patients.

Xinshuo Huang and Baoming Liang have contributed equally to this work.

✉ Hui-jiuan Chen
chenhuix5@mail.sysu.edu.cn

✉ Xi Xie
xiexi27@mail.sysu.edu.cn

1 State Key Laboratory of Optoelectronic Materials and Technologies, School of Electronics and Information Technology, Guangdong Province Key Laboratory of Display Material and Technology, Sun Yat-Sen University, Guangzhou 510006, China

2 School of Biomedical Engineering, Sun Yat-Sen University, Shenzhen 518107, China

3 Pazhou Lab, Guangzhou 510330, China

4 The First Affiliated Hospital of Sun Yat-Sen University, Guangzhou 510006, China

Graphic abstract

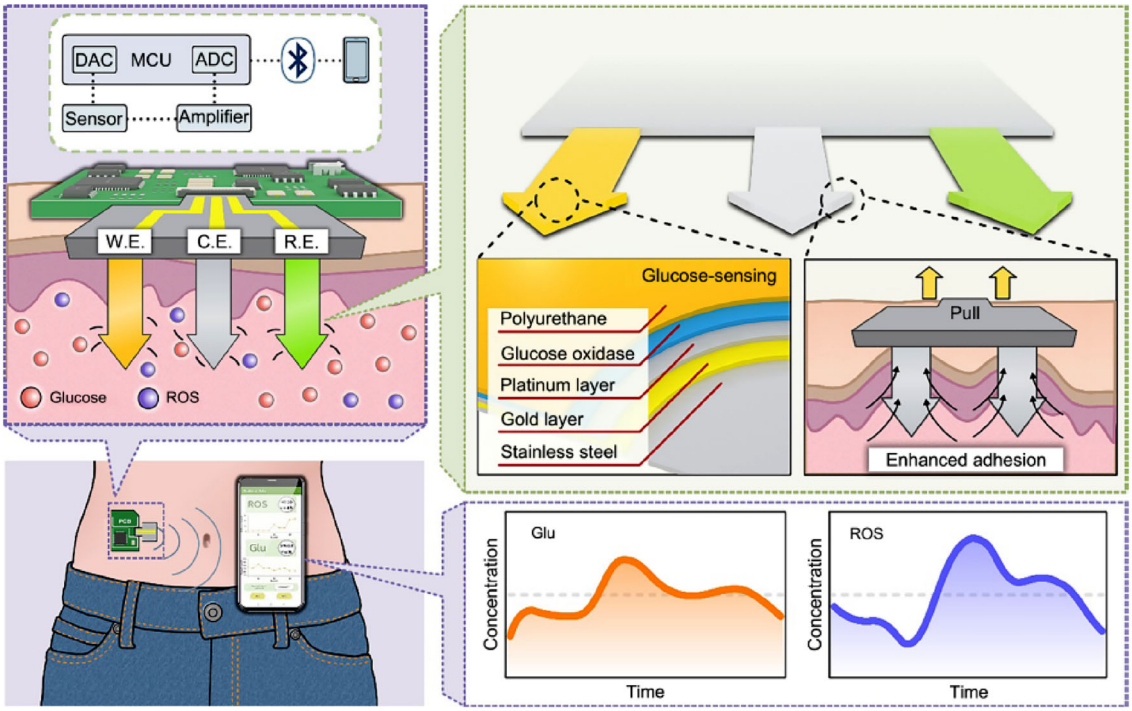

Keywords Microarrow sensor array · Glucose sensing · Reactive oxygen species sensing · Integrated system · Continuous monitoring

Introduction

Diabetes, a disease caused by high blood glucose levels due to insufficient pancreatic function in the body [1–3], gives rise to numerous complications that pose a threat to the heart, brain, eyes, kidneys, and other organs [4–6]. Researchers have developed a variety of strategies to diagnose diabetes [7–9], such as urine glucose testing, venous blood chemistry, fingertip blood glucose meters, ambulatory glucose meters, implantable glucose meters, and noninvasive glucose meters [10–12]. Unfortunately, the detection performances, such as sensitivity, stability, and requirement for repeated testing of these glucose-detection technologies, are still less than satisfactory with respect to improving our daily lives [13, 14]. Invasive methods are intended to improve sensitivity but are painful and inconvenient to use, with a potential risk of bacterial or viral infection and consequent disease transmission due to unavoidable wounds [15–17]. Consequently, noninvasive approaches have attracted significant attention from researchers in the recent past decade [18–20]. The collection and measurement of body fluids, including saliva, sweat, and tears, enabled the detection of specific biomarkers and facilitated the diagnosis and treatment of diseases [14, 21, 22]. However, the application of noninvasive approaches to body fluids is limited by the poor correlation of biomarkers between body fluids and blood vessels, which has not yet been proven [20, 23, 24].

Based on the frequent and close substance exchange between subcutaneous capillaries and intertissue fluid [25, 26], implantable electrodes have been developed as continuous glucose monitoring technology for clinical use [27–29]. However, the commonly used implantable electrodes were approximately 1 cm in length [30, 31], which could easily trigger subcutaneous inflammatory reactions as well as tissue fibrosis, introducing bias in the accuracy of detection. Moreover, the implantation of electrodes can be accompanied by pain, bleeding, and infection, reducing comfort and discouraging compliance in long-term wearing. These factors encouraged the development of microneedles, with needle lengths of 500–800 μm, which are capable of penetrating the dermis and epithelium with minimal invasiveness to directly reach the interstitial fluid without piercing the blood vessels or stinging the nerves, thereby avoiding painful sensations by the special miniatured needle structure [16, 32, 33]. Microneedles are widely used for detection and drug release because of their excellent minimal invasiveness and

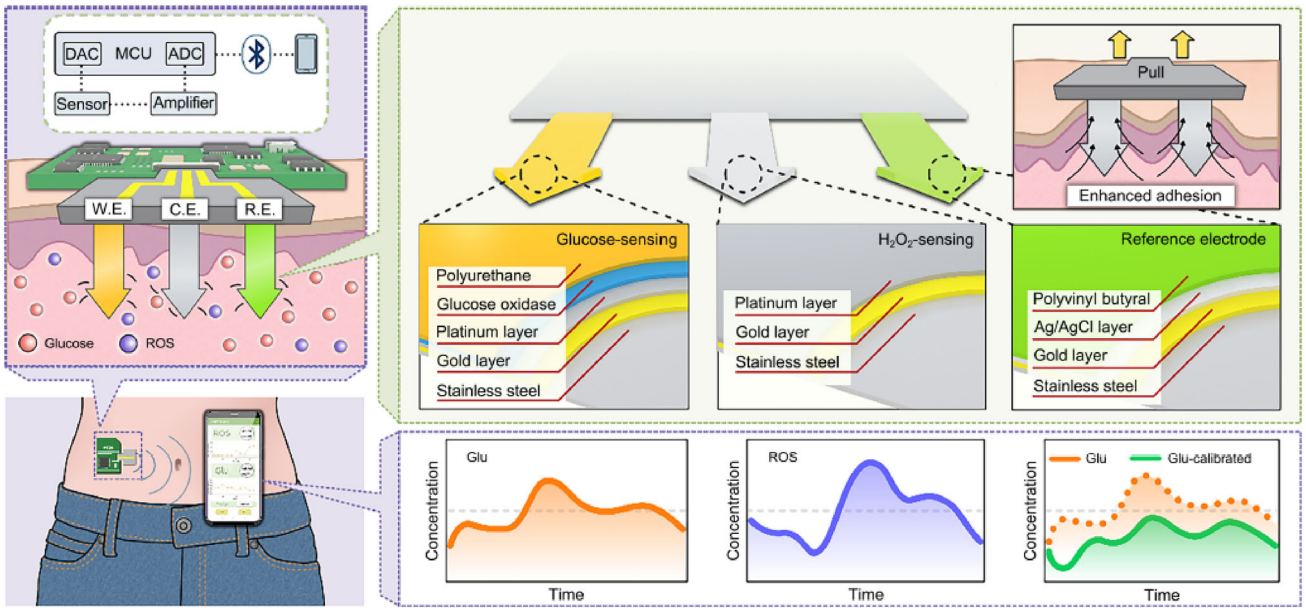

Fig. 1 Schematic diagram of the microarrow array system for the detection of H_2O_2 and glucose. The designed microarrow sensor array allowed for minimally invasive detection through the skin, where the concentration fluctuations of glucose and H_2O_2 in the subcutaneous tissue fluid were measured by a multilayer structurally modified microarrow sensing tip, after which the signals were transmitted to a microcontroller for processing through a printed circuit board, enabling specific and sensitive responses to different metabolites in the subcutaneous tissue fluid. DAC: digital-to-analog converter; MCU: microcontroller unit; ADC: analog-to-digital converter; W.E.: working electrode; C.E.: counter electrode; R.E.: reference electrode; ROS: reactive oxygen species; Glu: glucose

good biosafety, particularly in the field of diabetic diagnosis [34]. Reactive oxygen species (ROS) in living organisms are indicators of their health status as well as the progression of diseases. Diabetes is generally detected by the catalytic decomposition of glucose in the blood with the aid of glucose oxidase (GOx), which generates H_2O_2 for amperometric sensing. High concentrations of ROS in the body could raise the glucose signals measured during the detection process such that they deviate from the actual situation, causing sensing bias. The detection of the concentration of ROS in the in vivo environment would enable the understanding of the stage of inflammation that may interfere with glucose monitoring and result accuracy [35].

On the other hand, microneedles are prone to possess insufficient adhesion to skin and structural rebound in subsequent measurements due to the high elasticity of the skin and limited penetration depth of the microneedles [36, 37]. Moreover, adhesives based on chemical materials tend to cause skin irritation owing to their glue curing, degradation products, or low adhesion strength [38–40]. Inspired by the endoparasite, Yang et al. [41] developed a biphasic microneedle array that mechanically interlocks with tissue through swellable microneedle tips, achieving a 3.5-fold increase in adhesion strength compared with staples in skin graft fixation, providing universal soft tissue adhesion with minimal damage, less traumatic removal, and a reduced risk of infection. Similarly, Han et al. [42] reported a bioinspired, digitally light processing three-dimensional (3D) printing fabricated microneedle with backwards-facing barbs. The tissue adhesion of the backwards-facing barbed microneedle is 18 times stronger than that of the barbless microneedle, enabling sustained drug release in the tissue as well, demonstrating the potential of the structure in drug delivery, biofluid collection, and biosensing. For functional microneedle sensors, the development of microneedles with specialized tip morphologies is more challenging due to the difficulties of 3D fabrication of conductive microneedle materials and the need to avoid interference with the sensor module [43].

In this work, we developed an arrow-shaped microneedle (microarrow) sensor array (MASA), which offered enhanced adhesion to the surface and achieved simultaneous detection of glucose and ROS in interstitial fluid in vivo (Fig. 1). A planar steel sheet of microarrows was fabricated using laser micromachining, which was further modified with a functional coating and integrated into a patch of a 3D microneedle array with arrow-like tips. Due to the mechanical interlocking of the arrow tip with the tissue, the MASA adhered firmly to the skin surface after penetrating the skin. The microarrow sensor could detect various concentrations of glucose and H_2O_2 (representative of ROS) with sufficient sensitivity, and the detection displayed an excellent linear response range, reproducibility, and stability. Continuous in vivo monitoring of both glucose and H_2O_2 concentrations by the microarrow sensor was demonstrated, with the detection of H_2O_2

providing a valuable reference to evaluate the inflammation state during microneedle glucose detection. The MASA was integrated into a wearable monitoring system using a customized circuit. This work offered a promising tool for the reliable continuous monitoring of glucose fluctuation, which would facilitate the development of a closed-loop system for the automatic treatment of diabetic patients.

Experimental section

All of the following chemicals were purchased from Sigma–Aldrich (Guangzhou, China): NaCl, KCl, $CaCl_2$, $MgCl_2$, tetrahydrofuran, dimethyl formamide, polyurethane, 3% hydrogen peroxide, bovine serum albumin (BSA), glutaraldehyde solution (2%–2.5%), GOx, poly(vinyl butyral) resin BUTVAR B-98 (PVB), and phosphate buffered saline (PBS) (pH=7.2). The following chemicals were purchased from Yuncaitaotao Company (Huizhou, China): gold sulfite solution, platinum sulfite solution, and Ag/AgCl ink. All of the chemicals were used as received without further purification. All solutions were prepared using deionized water produced by Millipore Water Purification Systems unless otherwise noted.

Design of the microneedle structure

Based on SUS304 stainless steel, the microneedles were designed as a sheet structure, each with a length, width, and thickness of 12, 3, and 0.2 mm, respectively, with five protruding microneedles attached to the center of the long side, each approximately 800 μm long and 400 μm wide. The tip of each of the microarrows was machined with a pinch angle of approximately 30° and a microarrow structure on both sides of the needle tip, with each barb angle showing a sharp arrowhead with an exposed edge of approximately 20 μm. To integrate the preparation into a prototype effectively, a long shank of approximately 1540 μm for bending was added to the back of the microneedle sheet. The shank was folded at 90° in the subsequent preparation before combining the microneedles side-by-side to form a 4×5 microarrow array, which facilitated integration with the printed circuit board (PCB) through the PCB interface, ensuring the stable and continuous detection of glucose and H_2O_2 concentrations.

Fabrication of the microarrow electrode

Stainless steel (SUS304) with a thickness of 200 μm was cleaned and dried using ethanol according to the design process shown in Fig. 2a. A microarrow electrode with a conductive lead was cut using a laser machine, after which the lead of the microarrow electrode was bent at 90°, degreased, and washed. A YLP-F series optical fiber laser marking machine was utilized during the fabrication, with the following conditions: laser wavelength 1.06 μm, engraving line speed 1500 mm/s, power 18 W, and engraving 1200 times. The microarrow electrodes could also be fabricated by Huasheng Precision Hardware Co., Ltd. (Shenzhen, China). The oxidized layer on the surface was removed using acidic detergent, followed by the formation of a protective layer via electrochemical Au plating by electrochemical plating for 720 s with a current of 20 mA. The acidic detergent contained 24% zinc oxide, 30% ammonium chloride, 6% hydrochloric acid, 30% acetic acid, 12% deionized water, and 3% surfactant, and was provided by the company Yuncaitaotao. After modification, a microarrow electrode array was formed by integrating the electrodes with polydimethylsiloxane (PDMS).

Preparation of microarrow sensing electrodes

The H_2O_2-sensing microarrow electrode was prepared by the electrochemical deposition of Pt on the gold-coated electrode in platinum sulfite solution at a voltage of −0.3 V for 300 s to enhance the H_2O_2 response. The electrode was washed with deionized water and dried. For glucose sensing, 500 mL BSA (80 mg/mL), 200 mL glutaraldehyde solution (2.5%), and 100 mL GOx (50 mg/mL) were mixed and shaken for 30 min on a shaker to decorate the microarrow glucose-sensing electrode. The platinum-coated microarrow electrode was coated with the mixture using the dip-coating technique and dried overnight in an ambient environment. This was followed by further dip coating in a mixture comprising 9.8 mL tetrahydrofuran, 0.2 mL dimethyl formamide, and 0.4 g polyurethane to limit the transmission efficiency and allowed to dry overnight, at which point they were ready for testing. All the microarrow electrodes were stored in a sealed container at 4 °C when not in use.

Fabrication of the reference electrode

A piece of laser-cut microarrow electrode was immersed in acidic detergent and ultrasonically soaked for 5 h. It was then washed with 75% alcohol, wiped dry, and plated in gold sulfite solution at −20 mA for 1200 s. After ultrasonic soaking in 75% alcohol for 5 min, the sample was dried and uniformly coated with silver chloride ink before drying at 90 °C for 1 h. The prepared microarrow reference electrode was then dipped into PVB solution using an immersion coating method and dried at room temperature for 12 h whereupon they were ready for testing.

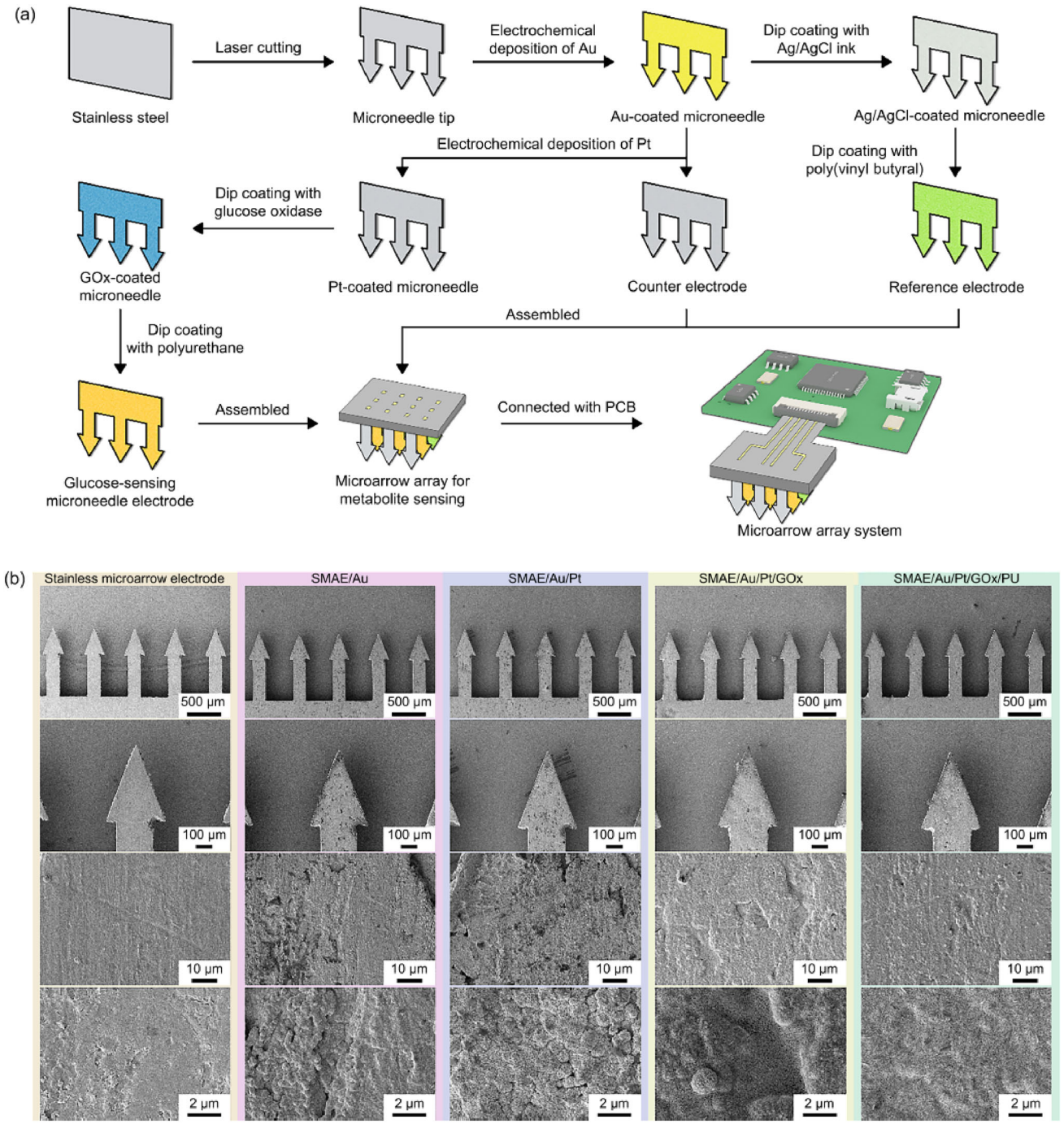

Fig. 2 Fabrication of the microarrow array system and characterization of microarrow electrodes. **a** Fabrication of the microarrow array. Planar steel was processed into a planar microarrow structure through laser cutting before a conductive gold layer was deposited on the microarrow tip by electrochemical reaction, followed by electrochemical deposition of a platinum layer for the sensing of H_2O_2 concentration. Furthermore, coating modifications of glucose oxidase (GOx) and polyurethane (PU) layers were performed on the microarrow electrode for glucose sensing. These microarrow working electrodes formed above were utilized for the selective measurement of glucose and H_2O_2 concentrations. In addition, the microarrow electrodes coated with an electrochemically deposited conductive gold layer were further modified with Ag/AgCl ink as well as a poly(vinyl butyral) resin BUTVAR B-98 (PVB) protective layer to form a reference electrode. The three microarrow patches (the working electrodes for glucose and H_2O_2 concentration sensing) and the microarrow reference electrode were integrated to form the microarrow sensor array (MASA), which could be further integrated with the printed circuit board (PCB) to support the sensing function of the microarrow device. **b** Left to right: morphological characteristics of blank microarrow patches, with no coating (blank), Au layer, Au plating modified with Pt layer, GOx, and PU layer, respectively

Assembly of electrodes into a microarrow array prototype

After the preparation of each patch of working electrodes and the reference electrode, the microarrow electrodes were then arranged in parallel at 3 mm intervals, combined with a 12 mm × 12 mm acrylic plate that was designed by software and processed by an engraved laser to form the MASA. The other parts of the microarrow electrodes were then covered with PDMS for insulation, after which the ends of the leads were trimmed uniformly and easily connected to the PCB interface to integrate the prototype.

Characterization with scanning electron microscopy (SEM)

Phenom Scientific Desktop SEM Pro (SUPRA 60, Wavetest) was used to characterize the surface morphology of the as-prepared microarrow electrodes and the modified microarrow electrodes. Owing to the limited conductivity of the microarrow electrode with the modified multilayer film structure, we deposited a layer of gold approximately 10 nm thick on the surface of the microarrow electrodes for improved observation.

Assessment of the penetration of porcine skin via fluorescence characterization

An aqueous solution of rhodamine B (2 mg/mL) was prepared, and a cotton swab was used to absorb a small amount of the solution and drop it on the head of the microarrow electrode to evenly stain the surface of the microarrow electrode tip. A piece of fresh porcine skin, utilized as a substitute for human skin, was cleaned by removing the grease from the surface and placed flat on a piece of foam. A microarrow electrode tip was positioned perpendicular to the surface of the porcine skin, propelled into the skin with force and allowed to stand for 4 min before the needle was pulled out. The porcine skin was subsequently observed using an optical microscope. Additionally, to demonstrate the transdermal performance of the microarrow electrode tip, a thin slice (with an approximately 200 μm) of the porcine skin that had been subjected to transdermal penetration was dissected along the cross section of the hole left by the microarrow electrode using a razor blade. The skin was then placed under a fluorescence microscope for observation of the red fluorescence.

Puncture force characterization

In vitro experiments were performed using porcine skin as a simulation of human skin. The microarrow electrode tip was fixed vertically downwards on the fixture of the puncture force measurement machine and placed vertically directly above the fixed skin. Then, the microarrow electrode tip was pressed vertically onto the surface of the fresh porcine skin by applying pressure from top to bottom, with a moving rate of 3 mm/s until lancing into the pig skin. After standing for 20 s, the tip was removed along the original path until the microarrow electrode was completely separated from the skin, during which the changes in the penetration force were recorded with a penetration force measurement machine to verify the adhesion of the microstructure of the microarrows, while the entire process of needle entry and detachment from the skin was recorded with a camera (α6300, Canon (China) Ltd.) for instant and visual observation.

Microarrow electrode in vitro sensing characterization

This experiment was conducted by placing the solution in a 25 mL beaker covered with a four-fold cling film to simulate the skin. A metabolite sensing microarrow array was used to puncture the cling film to simulate skin penetration, such that the microarrow electrode was fully exposed to the solution to detect glucose and H_2O_2 concentrations in the solution. A series of electrochemical characterizations were performed using a CHI 760E workstation (CH Instruments Inc., Shanghai, China) using a commercial Ag/AgCl electrode in combination with a commercial Pt counter electrode to evaluate the performance of the working electrodes. A three-electrode system was used to record the response of the metabolite sensor to PBS. The potential scan of the microarrow glucose-sensing electrode was scanned with a modified working electrode as the working electrode, a commercial platinum electrode as the counter electrode, and the Ag/AgCl electrode as the reference electrode. The electrodes were immersed in 10 mL of PBS solution in the beaker, and the cyclic voltammograms were recorded with CHI 760E software in the range of −0.4 to 0.8 V at a scan rate of 0.1 V/s. The potential of the H_2O_2-sensing electrode was scanned using a modified working electrode as the working electrode, a commercial platinum electrode as the counter electrode, and a Ag/AgCl electrode as the reference electrode. The electrodes were immersed in 10 mL of PBS solution in the beaker, and the cyclic voltammograms were recorded with CHI 760E software in the range of −0.4 to 0.8 V at a scan rate of 0.1 V/s.

Using a microarrow metabolite-sensing electrode as the working electrode, a commercial platinum electrode as the counter electrode, and a commercial Ag/AgCl electrode as a reference electrode, step response tests were performed on all metabolite sensors by applying a voltage (0.5 V for glucose sensing and −0.5 V for H_2O_2 sensing) to the three-channel system to evaluate their linear response capability for each subject over a specific range. For the detection of glucose, the concentration of glucose in the solution increased

gradually from 3 to 6, 9, 12, and 18 mmol/L, while the amperometric response of the electrode gradually increased with increasing glucose concentration. During these experiments, measurements were paused for 30 s each time the solution was changed to allow for complete diffusion of the solute in the solution. Similarly, H_2O_2 was detected by gradually increasing the concentration of H_2O_2 in the solution from 0 to 2, 4, 6, 8, and 10 mmol/L.

In vivo experiments

In vivo experiments were conducted using rats to evaluate the role of MASA in animal monitoring. The study was approved by the Institutional Animal Care and Use Committee of Sun Yat-Sen University. All animals received humane care in accordance with institutional guidelines. Sprague Dawley (SD) rats were obtained from the Sun Yat-Sen University Animal Facility and used for experimental studies. The animals used included two healthy rats and one diabetic rat. First, the rats were anaesthetized with gas, and an area of 4 cm×4 cm was depilated using surgical scissors and depilatory cream. Subsequently, the MASA was positioned over the depilated area such that the microarrow electrodes penetrated the skin. Care was taken to ensure that the MASA was in close contact with the skin and penetrated the stratum corneum. The amperometric detection by the metabolite-sensing microarrow electrode was recorded, and measurements were taken every 30 min for 3 h. In this study, we performed parallel experiments with three rats. The amperometric data measured by the MASA were converted into the concentrations of glucose and H_2O_2 according to the standard curve of the amperometric metabolite concentrations of the MASA. Blood was also collected from the tail artery of the rats every 30 min before using a biochemical analyzer to determine the concentrations of glucose and H_2O_2 in the blood as a reference value. The glucose levels in the blood collected from the rats were measured using a glucose meter (Roche, Ltd.), while the serum was analyzed using an H_2O_2 kit (Qiyun Biotechnology Co., Ltd., Guangzhou, China). Then, the rats were placed in their cages and observed to determine whether they engaged in normal activity.

Fabrication of printed circuit board

The PCB was designed and wired by an auto designer, after which it was then printed and aligned for soldering. After connecting the electrodes through the sensor interface, the board was powered by the battery module to collect potentiometric signals from the surface of the metabolite-sensing microarrow electrode and process them through a two-stage differential circuit to reduce signal distortion and common mode noise interference. Subsequently, the collected analog signal was converted into a digital signal by the STM32 chip through an analog-to-digital converter (ADC), and a gradient conversion was performed according to the calibration curve obtained from in vitro experiments to obtain the corresponding metabolite concentration. The result was transmitted to the Bluetooth module via a serial port to send the concentration data of different metabolites to the mobile terminal to display the graph showing the changes in the metabolite levels on the interface designed using Android Studio software.

Results and discussion

The fabrication process of the microarrow array is illustrated in Fig. 2a. First, the structural pattern of the microneedle sheet, designed using AutoCAD software, was transferred to a stainless-steel sheet with a laser-marking machine to prepare microneedles with a length of 800 μm. Each microneedle sheet contained five isolated microneedles, with a thickness of each microneedle of approximately 200 μm. The head of each microneedle was arrow-shaped, with a sharp angle of 30° at each end of the barbs, facilitating adhesion of the device to the skin surface after puncture. The stainless-steel microarrows were immersed in a gold sulfite solution for electroplating. By using an applied voltage of −0.8 V, a gold layer was electrochemically deposited uniformly on the surface of the microarrows to improve the electrode stability, biocompatibility, and corrosion resistance in the solution. For the detection of H_2O_2, voltages of approximately −0.3 V were applied in platinum sulfite solution to electrochemically deposit a platinum layer on the surface of the microarrows to further improve the stability of the electrode in the solution, enhancing the sensitivity of the electrode to H_2O_2. Meanwhile, the presence of the platinum layer facilitated the resistance to corrosion by oxygen and voltage in solution and served to protect the microarrow sensing electrode. Furthermore, to specifically detect glucose concentration in the interstitial fluid, GOx was deposited on the surface of the Pt electrode using dip coating to selectively convert glucose into H_2O_2, which enabled the glucose concentration in solution to be correlated with the H_2O_2 concentration by exploiting the electrochemical response of the electrode to H_2O_2 concentration. This in turn allowed the fluctuations in the glucose level in the interstitial fluid to be detected.

Electrochemical detection was based on microarrow electrodes with progressively deposited gold and platinum layers serving as counter electrodes. The microarrow reference electrode was prepared as described previously. The surface of this microarrow reference electrode was modified by dip coating with PVB to slow the oxidation of Ag and improve the stability of the reference electrode. The protective PVB

layer served to stabilize the potential of the microarrow reference electrode, thereby markedly enhancing the immunity of the electrode signal to changes in the chloride concentration in the environment, which improved the stability of the signal to ultimately enhance the detection accuracy.

The microarrow electrodes described above were then arranged, bonded, and assembled in the form of a 3D microarrow array with a tip spacing of 3 mm within a 3-mm-thick PDMS layer. These three microarrow working electrodes were utilized for metabolite detection. The surface morphology of the multiple-layer microarrow electrodes during fabrication was characterized using SEM. As shown in Fig. 2b, the stainless-steel and gold-coated microarrow electrodes possessed smooth and uniform surface morphologies. In contrast, after platinum plating and coating with the GOx membrane, the surface of the microarrow electrodes exhibited the corresponding layer morphology. The polyurethane coating resulted in an uneven morphology with nodule-like protrusions, which lowered the transmission efficiency of glucose. Finally, a 5-mm-thick microarrow device was formed by bending the conductive leads on the substrate of the microarrow sheet for a more effective connection with the PCB.

The as-prepared microarrow sensing electrodes were tested in an in vitro simulated solution. A polyvinyl chloride (PVC) film was utilized to simulate the skin cuticle, which was placed on top of the solution. The microarrow electrodes penetrated the film such that the tip of the electrodes extended into the solution below the film for testing. In general, the glucose concentration of a healthy human ranges from 3.3 to 6.9 mmol/L, and the H_2O_2 concentration in the human body is less than 1 mmol/L. Testing the MASA in vivo required a wider concentration range that included the above substrate concentration range; e.g., glucose was tested in the range of 3–18 mmol/L, and H_2O_2 was tested in the range of 0–10 mmol/L. For the detection of H_2O_2, the concentration was varied gradually from 0 to 10 mmol/L in the aqueous solution tested in vitro. By applying a certain negative bias (−0.5 V vs. Ag/AgCl, which was obtained through a cyclic voltammetry test, Fig. S1 in Supplementary Information) to the surface of the microarrow platinum electrode, the decomposition of H_2O_2 was produced on the surface of the electrodes, generating electrons that form an electrical signal and flow through the electrode surface to the electrode interior. This formed an amperometric loop, through which the H_2O_2 in solution was converted into an electrical signal, and the subcutaneous H_2O_2 concentration was converted into a measurable amperometric signal and correlated with the corresponding ROS concentration. As shown in Fig. 3a, as the H_2O_2 concentration gradually increased from 0 to 10 mmol/L, the amperometric detected by the microarrow electrode also gradually increased from −110 to −460 μA. A linear fit of the amperometric signal to the H_2O_2 concentration revealed a linear relationship between the amperometric signal of the microarrow electrode and the H_2O_2 concentration with an average sensitivity of 35.45 $\mu A \cdot mmol^{-1} \cdot L^{-1}$.

To facilitate the mass production of microarrow array sensors and to verify their potential for repeated applications, the reproducibility of different H_2O_2-sensing microarrow electrodes was evaluated. Five batches of H_2O_2-sensing microarrow electrodes were prepared and used in parallel to analyze the test solution. As shown in Fig. 3b, a comparison of the responses of five H_2O_2-sensing microarrow electrodes from different batches revealed that the same type of sensor showed a similar trend with increasing substrate concentration and operated with a similar sensitivity (approximately 10% error). Additionally, the stability of the H_2O_2-sensing microneedle electrodes was investigated, and the performance after storage was explored after fabrication. Figure 3c shows the changes in the daily sensitivity of each microarrow electrode over five days, where the sensitivity changes were calibrated for each subsequent day by testing different electrodes and setting sensitivity on the first day to 100% as the base value (the absolute value of sensitivity over storage time is shown in Fig. S2 in Supplementary Information). The results showed that the H_2O_2-sensing microarrow electrode maintained excellent temporal stability over four days and still maintained a sensitivity of approximately 80% after five days. Apart from this, the coexistence of multiple biomarkers for metabolite detection may be disturbed after integrating the microarrow metabolite-sensing electrodes into the MASA. Therefore, the selectivity of the metabolite-sensing sensor was evaluated using the corresponding markers. Figures 3d and S3 (Supplementary Information) depict the response of the H_2O_2-sensing microarrow electrode to the target and interfering substances during continuous monitoring. The test was performed by sequentially adding lactic acid, potassium chloride (as a representative salt), cholesterol, ascorbic acid, and uric acid to the test solution used to test the H_2O_2-sensing microarrow electrode. The results showed that this microarrow electrode detected a significant amperometric signal only in the presence of H_2O_2, whereas the presence of interfering substances produced only a weak amperometric signal (<8%) to the electrode, demonstrating that the H_2O_2-sensing microarrow electrode could selectively detect H_2O_2 and was not affected by interference from other interfering substances.

For the testing of blood glucose levels in vitro, the concentration of the aqueous solution was varied gradually from 3 to 18 mmol/L. Assisted by oxygen, GOx was able to selectively catalyze the decomposition of glucose in solution, producing gluconic anhydride and H_2O_2. By applying a certain positive bias (0.5 V vs. Ag/AgCl) to the surface of the platinum microarrow electrode, the generated H_2O_2 was catalytically decomposed, followed by electron transfer, after which the

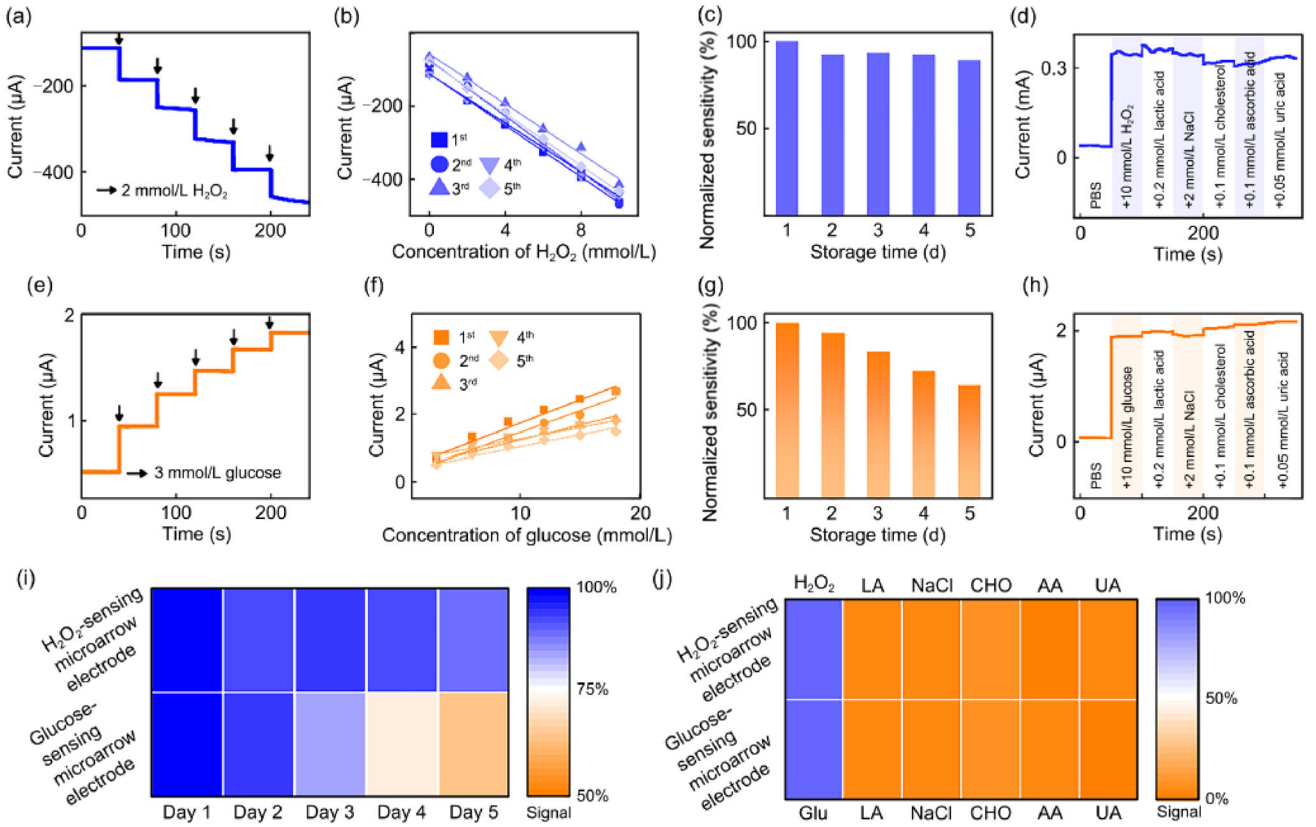

Fig. 3 Characterization of microarrow electrodes. **a** Linear response of the H_2O_2-sensing microarrow electrode to different concentrations of H_2O_2 (0–10 mmol/L). **b** Parallel experiments to test the response of five H_2O_2-sensing microarrow electrodes to detect different concentrations of H_2O_2. **c** Statistical analysis of the stability of the linear response of the H_2O_2-sensing microarrow electrode to detect different concentrations of H_2O_2 detected over five days, expressed as normalized values. **d** Specific response of the H_2O_2-sensing microarrow electrode to H_2O_2, with changes in response amperometric related to the presence of lactic acid (LA), sodium chloride (NaCl), cholesterol (CHO), ascorbic acid (AA), and uric acid (UA), respectively. **e** Linear response of the glucose-sensing microarrow electrode to detect different concentrations of glucose from 3 to 18 mmol/L. **f** Parallel experiments of the linear response of glucose-sensing microarrow electrodes to the glucose concentration. **g** Statistical analysis of the stability of the linear response of the glucose-sensing microarrow electrode to the glucose concentration over five days, expressed as normalized values. **h** Specific response of the glucose-sensing microarrow electrode to glucose concentration, with changes in the response amperometric related to the presence of lactic acid, sodium chloride, cholesterol, ascorbic acid, and uric acid, respectively. **i** Comparison of the temporal stability of the H_2O_2-sensing microarrow electrode with that of the glucose-sensing electrode and summarized as a heatmap. In this case, the final relative sensitivity of the H_2O_2-sensing microarrow electrode remained above 80% after five days of utilization. Similarly, the final relative sensitivity of the glucose-sensing electrode was close to 70% after five days of usage. **j** The detection selectivity of the two types of microarrow sensing electrodes was summarized as a heatmap with the interference signal normalized to the target detection signal. PBS: phosphate buffered saline; Glu: glucose

generated electrical signal flowed through the electrode surface to the interior of the electrode, forming an amperometric loop. In this way, the glucose in solution was converted into H_2O_2, and an amperometric signal was generated, converting the unmeasurable glucose concentration into a measurable signal. The amperometric signal between the microarrow working electrode and the reference electrode was measured by applying a forwards bias voltage (0.5 V) between the working electrode and the reference electrode, which was further correlated with the corresponding glucose concentration.

As shown in Fig. 3e, the gradual increase in glucose concentration from 3 to 18 mmol/L was accompanied by a gradual increase in the amperometric signal from 0.54 to 1.84 μA. A linear fit of the amperometric signal to the glucose concentration revealed a linear relationship between the amperometric signal of the microarrow electrode and the glucose concentration with an average sensitivity of 89.43 $\mu A \cdot mmol^{-1} \cdot L^{-1}$. A similar approach was utilized to evaluate the reproducibility of different microarrow glucose-sensing electrodes. Five batches of microarrow glucose-sensing electrodes were prepared and tested in parallel. Figure 3f compared the sensing responses of the five microarrow glucose-sensing electrodes, which indicated that the glucose-sensing electrodes exhibited similar trends with increasing

substrate concentration and operated with similar sensitivity (an error of approximately 30%). The stability of the glucose-sensing microarrow electrode was also investigated, as shown in Fig. 3g, by conducting a daily sensitivity test for five days, with the sensitivity on the first day set to 100% as the base value and calibrated for sensitivity changes on each subsequent day. The results suggested that the microarrow glucose-sensing electrode maintained excellent temporal stability over five days and maintained a sensitivity close to 70% after five days. The decrease in sensitivity was mainly due to the degradation of glucose oxidase coated on the microneedle during the storage period. In practical applications, the enzyme activity of glucose oxidase could be better preserved by storage of microneedles at lower temperatures or even in noble gas environments. Moreover, the stability of the electrode can be improved by adding or optimizing the outer membrane (e.g., Nafion or PU membrane) on the electrode to protect the enzyme layer. The enzyme stability of glucose oxidase could also be improved by designing more optimized enzymes through synthetic biology methods or using inorganic nanoenzymes so that the enzyme degradation issue could be better avoided.

In addition, evaluation of detection selectivity was demonstrated, as shown in Fig. 3h, where lactic acid, potassium chloride (as a representative salt), cholesterol, ascorbic acid, and uric acid were added sequentially to the test solution during in vitro detection by the glucose-sensing microarrow electrode. The results showed that the microarrow glucose-sensing electrode possessed specific detection performance for glucose concentration. For the detection of glucose, the microneedle sensor was based on glucose oxidase, which selectively catalyzed the decomposition of glucose in the blood to produce H_2O_2, and H_2O_2 was further detected by applying a bias voltage to decompose H_2O_2 at the microneedle electrode. Since glucose oxidase can only catalyze the oxidation of glucose specifically, theoretically, the sensor would rarely respond to other molecular substances, such as fructose, galactose, lactic acid, uric acid or ascorbic acid, as we tested. Furthermore, the results in Figs. 3i and 3j showed the temporal stability and specificity of the H_2O_2 and the microarrow glucose-sensing electrodes. These results were summarized in the form of a heatmap plot, where the corresponding sensing signals were normalized. The results indicated that the glucose-sensing microarrow electrode exhibited a significant amperometric signal only in the presence of glucose, whereas the presence of interfering substances produced only a weak amperometric signal (<10%) to the microarrow electrode, thus demonstrating that the glucose-sensing microarrow electrode could selectively detect glucose levels without being affected by interfering substances. The above results suggested that for the MASA, each interfering substance generated less than 10% of the interference signal, which indicated that the MASA could potentially monitor the corresponding metabolites in complex environments, such as in sweat, tears, or interstitial fluids. These results demonstrated that the as-prepared microarrow electrode could sensitively and selectively detect the concentration changes of the target metabolite across a good linear range, consistent with the detection range for in vivo application. To ensure that the continuous monitoring was sufficiently accurate, electrochemical sensing data were acquired for a period of 120 s for signal stabilization.

To characterize the ability of the microarrow to penetrate skin, in vitro experiments were conducted using porcine skin for simulation. First, the blank microarrow tips were stained with rhodamine B displaying red fluorescence, after which excess stain was removed. Then, microarrow tips were positioned above the surface of fresh porcine skin and inserted perpendicularly by applying pressure on the top. After standing for 4 min, the tips were removed, and the microaarrow-treated porcine skin was observed under optical and fluorescence microscopy. As shown in Fig. 4a, the tissue surrounding the positions where the surface of the porcine skin was penetrated by the microarrows emitted red fluorescence, confirming successful penetration of microarrows in the skin. Clear deposition of fluorescent dye was observed in the cross-sectional view of the fluorescence microscopic image, consistent with the morphologies of the microarrow in the skin penetration area. As shown in Fig. 4b, the maximum penetration depth of the microarrows was approximately 400 μm, which was shorter than the tip length of the microarrow (~800 μm). This was speculated to be caused by either the curvature of the skin or the elasticity of the skin that caused rebounding of the microarrow. Nevertheless, the penetration depth of the microarrow tips was on average 200–300 μm, which extended beyond the total thickness of the human stratum corneum (10–15 μm) and epidermis (50–100 μm) layers. This verified the ability of the microarrow tips to penetrate the skin layer.

To evaluate the ability of the microarrow structure to enhance adhesion into skin, the microarrows were tested in vitro using fresh porcine skin for simulation. First, the microarrow patch was clamped pointing vertically downwards in the mechanical test fixture, and fresh porcine skin was placed on the mechanical test platform. The software was set to drive the mechanical test fixture downwards slowly and evenly, ensuring that the microarrow tips penetrated the skin vertically and stopped at the maximum depth of the microarrows. The microarrow tips were left in the skin for 20 s to allow the skin to remove excess stress. Thereafter, the software was set to control the mechanical test fixture to slowly move upwards at the same speed to retract the microarrows upwards from the surface of the porcine skin (Fig. 4c). The changes in the forces on the different microarrow structures (Fig. 4d; red: with microarrows; black: without microarrows) before and after penetrating and being retracted from the skin

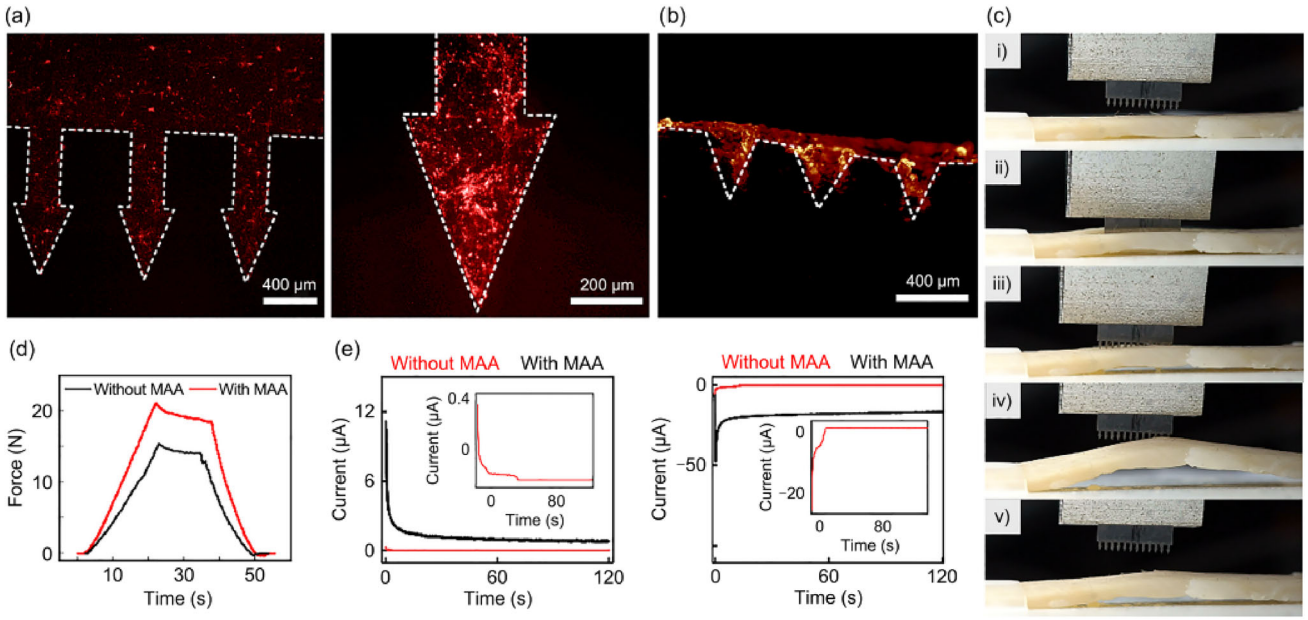

Fig. 4 Characterization of microarrows. **a** Fluorescence images of microarrow electrodes stained with rhodamine B at different magnifications. **b** Deposition of rhodamine B on porcine skin after penetration of microarrow electrodes. **c** Photographs showing the process of penetration and withdrawal from porcine skin via the microarrow electrodes with the structure of microarrows. **d** Curves showing the different responses and stresses of the microneedle array when applied to flat porcine skin with (red) and without (black) the microarrow structure. **e** Amperometric signal response of glucose-sensing microarrow electrode (left) and H_2O_2-sensing microarrow electrode (right) when attached to the back of rats in the absence (red) and in the presence (black) of microarrows during in vivo experiment. MAA: microarrow array

were recorded. A maximum force of approximately 20 N was observed, suggesting that the skin adhesion ability of the microarrow structure was higher than that of electrodes without the arrow structure.

The adhesion properties of electrodes with the microarrow structure were also tested in vivo. Specifically, by using microneedle arrays with and without microarrow structures for electrochemical sensing, in vivo experiments were carried out to evaluate the measurement performance of different metabolites. The microarrow electrode array sensor was attached to the skin of rats, and bias potentials (positive for glucose sensing and negative for H_2O_2 sensing) were applied through the electrochemical system to record the changes in the amperometric signal over time. As shown in Fig. 4e, although the microneedles without arrow tips could also detect electrochemical signals in vivo, the sensing signal was more prone to disappear during experiments since the sensor could more easily detach from the rat skin due to the body movement of the rat. On the other hand, because the barb structure adhered to the skin more effectively, the sensor with the microarrow structure recorded continuous amperometric signals after transdermal penetration with higher success rates in a more stable manner during experiments.

In vivo experiments were performed on rats to verify the performance of the MASA with respect to the detection of H_2O_2 and glucose fluctuations in interstitial fluids. The rats were anaesthetized, and the hair was removed from their dorsum. Then, the MASA was pressed against the skin on the rat's dorsum, allowing the microarrows to penetrate the stratum corneum. A bias voltage of 0.5 V was applied to the microarrow working electrode (vs. Ag/AgCl reference electrode, for the detection of H_2O_2, a bias voltage of −0.5 V was applied) to detect the amperometric signal between the working and counter electrodes of the sensor, and measurements were recorded every 30 min for 3 h. Parallel experiments were performed on three rats, including two healthy rats and one diabetic rat. The amperometric signal collected by the microarrow array sensor was used to derive the corresponding concentrations of H_2O_2 and glucose by converting the standard curve of the amperometric-substrate concentration of the MASA. Blood was collected from the tail arteries of the rat every 30 min, and the corresponding glucose concentration in the blood was determined using a commercial blood glucose meter as a reference to evaluate the sensor accuracy. The H_2O_2 concentration was determined via differential centrifugation of the collected arterial blood to obtain serum, and H_2O_2 indicator test paper was

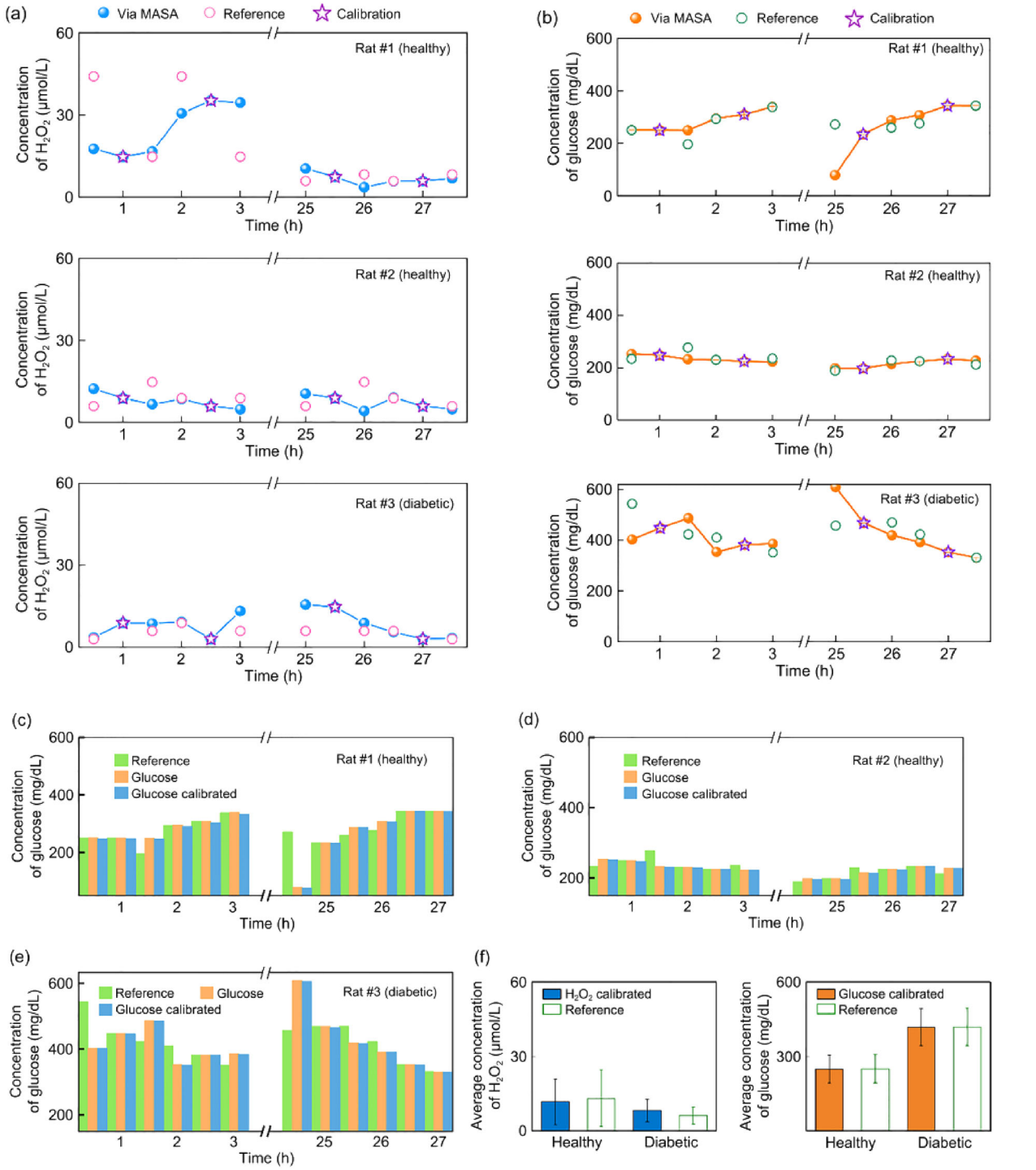

Fig. 5 In vivo continuous monitoring of rats using metabolite-sensing microarrow electrodes for 3 h**.** Transdermal penetration was performed by pressing the metabolite-sensing microarrow electrode against the dorsum of the rat. The amperometric signals of the concentration of two metabolites (**a** H_2O_2 and **b** glucose) detected by the microarrow electrode were recorded. The amperometric signals were converted into the corresponding metabolite concentrations according to the standard curve derived from in vitro tests. Reference concentrations of H_2O_2 and glucose in rat blood were measured at t=0.5 h using a commercial standard method, and the results recorded with the MASA were calibrated according to the reference concentrations (purple stars: calibration points; pink dots: reference H_2O_2 concentration; green dots: reference glucose concentration). **c–e** Glucose concentrations were calibrated using measured H_2O_2 concentrations, and the comparison of glucose levels with reference levels before and after calibration was performed for error reduction. **f** Measurement of H_2O_2 and glucose concentrations in healthy and diabetic rats for 2 days. Rat #1 and Rat #2 were healthy rats, and Rat #3 was a diabetic rat. Data were presented as mean±standard deviation (n=3)

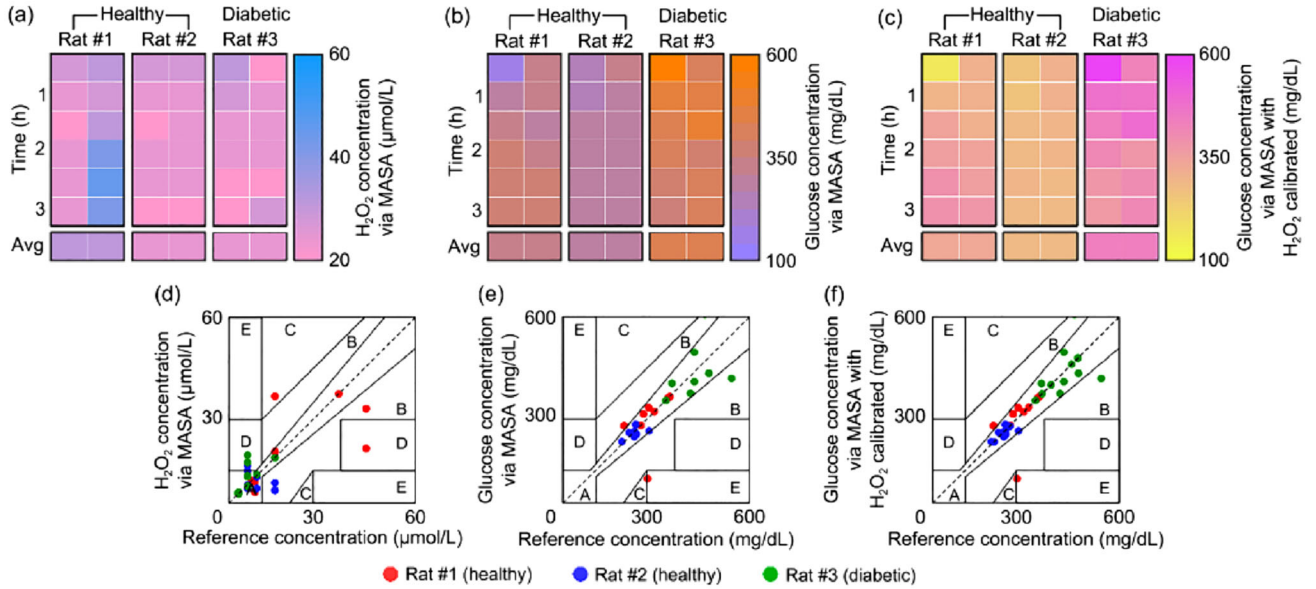

Fig. 6 Calibration and analysis of the sensing results of the MASA. Heatmap plots of fluctuations in biomarker concentrations in rats were measured by MASA, including **a** H_2O_2, **b** glucose, and **c** glucose concentrations calibrated by the measured H_2O_2 concentration. **d**–**f** Clarke's error grid analysis showing the detection accuracy of the MASA compared to the actual concentration during the sensing of **d** H_2O_2, **e** glucose concentrations, and **f** together with data calibrated with the H_2O_2 level. The calibration points were set at the second and second to last time points recorded considering the difference between the in vitro solution assay and the in vivo assay

utilized to detect H_2O_2 in the serum as a reference. Additionally, considering the differences between the in vitro solution assay and the in vivo assay, the substrate concentration measured at the second and second to last time points recorded was regarded as the calibration value for establishing the signal-concentration standard curve for the metabolite-sensing microarrow electrodes. Figures 5a and 5b show the variation in the concentrations of H_2O_2 and glucose detected by the MASA over two days. The blue and orange curves correspond to the concentrations measured by the metabolite-sensing microarrow electrodes, respectively, whereas the pink dots represent the reference H_2O_2 concentrations and the green dots represent the reference glucose concentrations. As shown in Fig. 5a, for the sensing of H_2O_2, the concentration fluctuations and errors in vivo were greater in Rat #1 on the first day and lower on the second day with smaller errors. For Rat #2 and Rat #3, there was little fluctuation in the concentration of H_2O_2 in the in vivo experiments, and the error was smaller. For the sensing of blood glucose, as shown in Fig. 5b, the blood glucose level of healthy rats did not exhibit large fluctuations in the 2-day in vivo experiment with a smaller error. For diabetic rats, the blood glucose level showed large changes on the first day of the experiment and smaller fluctuations on the second day, but the sensing results did not show large errors during the in vivo experiment.

Furthermore, the glucose concentration could be calibrated by subtracting the measured H_2O_2 concentration, as shown in Figs. 5c–5e and S4 (Supplementary Information). The measured H_2O_2 was utilized to calibrate the glucose concentration, and the glucose concentration was compared with the reference values, both before and after the calibration, to verify the correction effect of H_2O_2 during glucose sensing. Figure 5f displays the comparison of the average concentrations of H_2O_2 and glucose in both healthy and diabetic rats. For H_2O_2, the average H_2O_2 concentration appeared to be slightly higher in healthy rats than in diabetic rats. Notably, the average in vivo H_2O_2 concentration detected by the reference method and microarrow sensor was relatively small, at ~10 μmol/L, suggesting that the experimental rats were not in an obvious inflammatory state. For glucose sensing, the average glucose concentration of diabetic rats was higher and fluctuated more than that of healthy rats.

To better analyze the functionalities of H_2O_2 and blood glucose detection by the MASA, the concentrations of H_2O_2 (Fig. 6a) and glucose concentration without (Fig. 6b) or with calibration by the measured H_2O_2 concentration (Fig. 6c) were summarized in the form of a heatmap plot. Furthermore, the detection accuracy of H_2O_2 and blood glucose levels by the MASA was quantified and tested with Clarke's error grid analysis. For the detection of H_2O_2, the mean error was (32.5±40)% for Rat #1, (32.0±36.8)% for Rat #2, and (35.8±52.0)% for Rat #3 (Fig. 6d). In Clarke's error grid analysis, 80% of the data from Rat #1, Rat #2, and Rat #3 were located in zone A as well as zone B (sensing error<20%). For glucose detection, the error of the amperometric signal measured by MASA was less than 16%, with

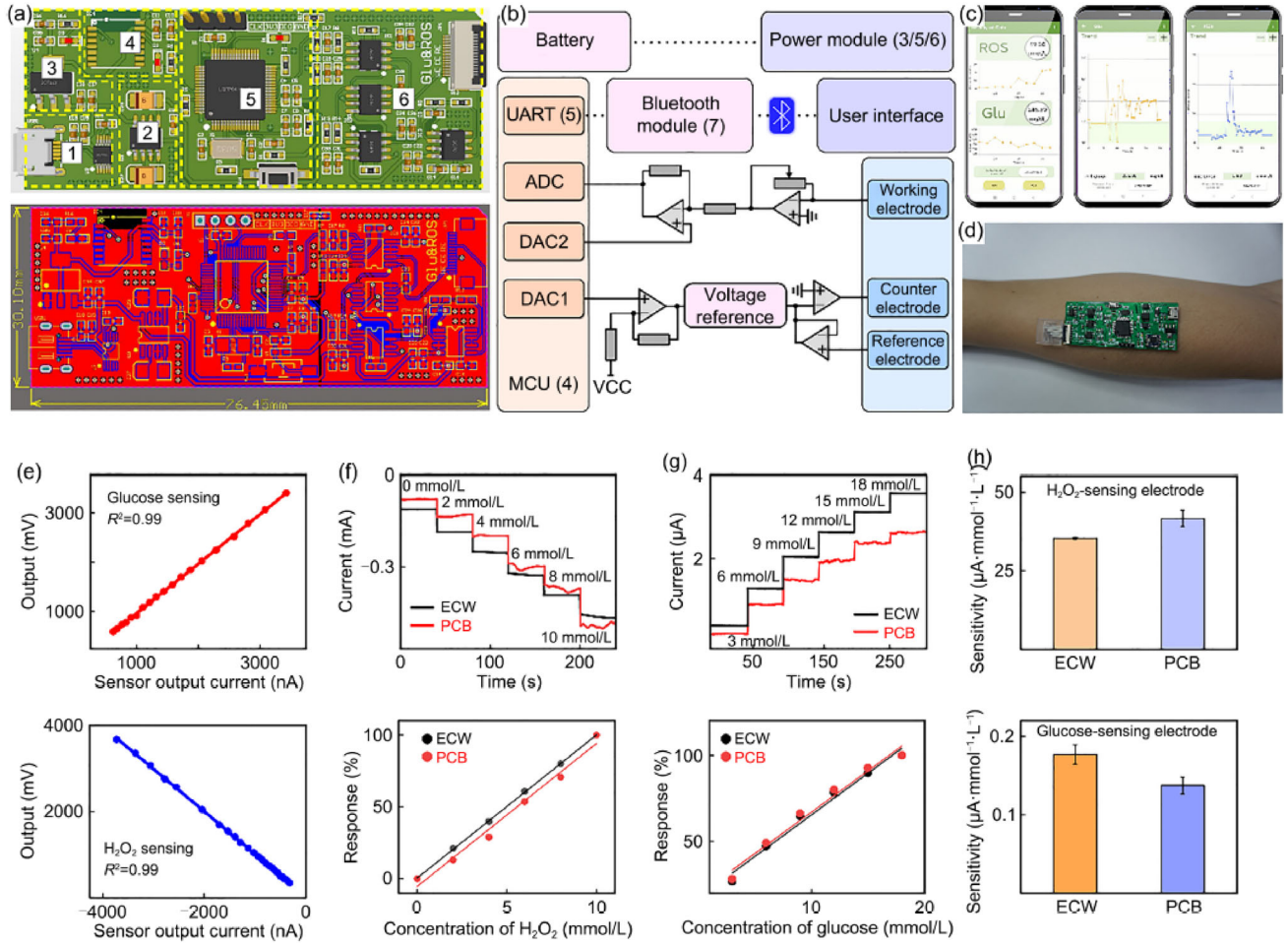

Fig. 7 Design and functional verification of supporting circuit board for the microarrow sensor array (MASA). **a** Circuit logic diagram (top) of the printed circuit board (PCB) and the system block diagram (bottom) of the supporting circuit for MASA. The yellow dashed boxes indicate the separate regions in which the circuit components and modules were located. The circuit module contained the required integrated circuit chips and peripheral electronics to record the amperometric signals corresponding to the glucose and H_2O_2 levels, as well as the signal processing, control and feedback, and Bluetooth wireless transmission circuitry. Thus, a compact system was formed by the module to support the functions of the microneedle device. The sensing circuit module consisted of two parallel sets of three-electrode systems for glucose and H_2O_2 concentration detection. The three-electrode system recorded the amperometric signals corresponding to the metabolite concentrations. **b** Circuit implementation and layout design diagram of the PCB. **c** User interface of the metabolite detection app, which communicates with the circuit module via Bluetooth transmission in real time. **d** Photograph of the PCB. **e** Signal calibration of the PCB for continuous and intermittent input and output voltage signals from −4 to 0 V (top) and voltage signals from 0 to 3.5 V (bottom), which could be utilized for amperometric detection of the concentration of H_2O_2 and glucose measurement, respectively. Amperometric signal response (top) from **f** the H_2O_2-sensing electrode and linearity of the amperometric (bottom) versus H_2O_2 concentration and **g** the glucose-sensing electrode and linearity of the amperometric (bottom) versus glucose concentration using the prepared PCB and a commercial electrochemical workstation (ECW). **h** Statistical results of the average sensitivity of the amperometric signal response of the sensor electrode to H_2O_2 (top) and glucose (bottom) levels measured using the as-prepared printed circuit board and ECW. UART: universal asynchronous receiver/transmitter; ADC: analog-to-digital converter; DAC: digital-to-analog converter; MCU: microcontroller unit

an average error of (10.2±20.0)% for Rat #1, (3.9±4.8)% for Rat #2, and (9.7±10.5)% for Rat #3 (Fig. 6e). In Clarke's error grid analysis, 87.5% of the data from Rat #1 and 100% of the data from Rat #2 and Rat #3 were located in zone A as well as zone B (sensing error<20%). Similar results appeared after the calibration of glucose with the detected H_2O_2 concentration (Fig. 6f). The actual concentration of H_2O_2 was low (below 30 μmol/L) in these rats, indicating that less inflammation occurred; thus, the presence of ROS did not significantly interfere with the detection accuracy of glucose concentration. Therefore, the calibration of glucose sensing by the concentration of ROS in the in vivo experiments did not further significantly enhance the microneedle glucose sensing accuracy. The difference between calibration with reactive oxygen correction might be more obviously

observed in animal models with stronger in vivo inflammatory responses. The calibration based on the H_2O_2 sensing results could further subtract this H_2O_2 background. The above results indicated that MASA could continuously monitor the concentration of H_2O_2 and glucose in the interstitial fluid when used as an in-situ sensor.

The entire diabetes detection system consisted of the MASA, a printed circuit board, and a software system. The glucose and H_2O_2 levels were detected using the MASA, which converted the subject concentration to an analog circuit signal through electrochemical reactions. A printed circuit that supported the function and operation of the MASA was developed. The microarrow patch was designed with extended leads as an interface for electrical connection to the PCB. The circuit diagrams used for signal conditioning, processing, and wireless transmission in MASA and their logical pathways were depicted in Figs. 7a and 7b, respectively, and details of the components of each module demarcated by the yellow lines were presented in Figs. S5–S10 (Supplementary Information). The circuit of the PCB contained a detection module to support the two sets of three-electrode sensors for glucose and H_2O_2 detection, where each set was capable of outputting stable bias potentials (positive and negative potentials for glucose detection and H_2O_2 detection, respectively) and recording the amperometric signals corresponding to the glucose and H_2O_2 concentrations in real time.

Analog signals were processed and sent to the microprogram control unit (MCU) and converted into digital signals via the ADC port of the microcontroller. The three-electrode modules ensured stable recording of the amperometric signals, which reflected the concentrations of glucose and H_2O_2 through time division multiplexing. The data output from the microcontroller could be transmitted to a smartphone application via a wireless transceiver for real-time observation. In addition, as shown in Figs. 7c and S11 (Supplementary Information), the smartphone app included a main interface (showing the metabolite levels) and subinterfaces (showing variations in the H_2O_2 and glucose levels over time). The interface enabled real-time monitoring of fluctuations in H_2O_2 and glucose levels, demonstrating that the circuit (Fig. 7d) and application may be utilized to support the MASA.

The linear accuracy of the acquisition and output signals of the PCB was characterized. The designed and prepared detection circuit generated amperometric signals under the application of a constant voltage of 0–3500 mV (−4000 to 0 mV for H_2O_2 sensing) and converted the current to the corresponding voltage signal through an AD5220 resistor chip; i.e., the voltage signal was recorded, and the corresponding output was obtained. The analog electrochemical signals of both channels were accurately conditioned, processed, and output (R^2=0.99). The stabilized voltage could be used as a bias potential and for electrochemical sensing of the MASA, as shown in Fig. 7e. The results obtained with the MASA for the detection of fluctuations in blood glucose and H_2O_2 concentration were consistent with those obtained using the commercial electrochemical workstation (ECW), both of which produced similar standard curves based on the signal concentration. Performance tests (Figs. 7f–7h; S12 and S13 in Supplementary Information) indicated that the PCB processed good linearity and high accuracy for the acquisition and output of signals, confirming its ability to maintain stable signal transmission. The analog electrochemical signals of the two three-electrode systems were precisely conditioned, processed, and delivered as output (R^2=0.99). These observations indicated a tight connection between the PCB and the sensor for stable signal acquisition and signal output and confirmed that this connection could be utilized for communication with a smartphone and perform metabolite sensing. In addition, the accuracy of the input and output could be linearly calibrated using software to eliminate errors such as amperometric drift and interference by foreign objects, thus improving the stability of the sensor.

The results showed that the designed printed circuit was capable of providing satisfactory amperometric output and signal recording to support the sensing function of the MASA. The tracking and detection of glucose and H_2O_2 fluctuations over an extended period of time was achieved by connecting the MASA to a PCB to form the system (total size 80 mm×35 mm×10 mm, mass ~15 g), demonstrating the potential of the MASA to track fluctuations in subcutaneous metabolite concentrations. Additionally, the universal serial bus (USB) interface of circuit was utilized for power supply currently for demo, which was not in the form of a wireless wearable device. However, the USB power could be further replaced by connecting to a 5-V lithium battery to increase the portability of the system, although the size and weight of the device needed to increase to accommodate the addition of battery. Owing to the combination of electronic circuits, the system could effectively support the operation and function of the MASA for real-time subcutaneous monitoring of bioanalytes.

Conclusions

In this work, we developed a microarrow sensor array with enhanced skin adhesion for continuous transdermal monitoring of glucose and H_2O_2 levels. The sensor included a microarrow array-based electrochemical sensor, corresponding printed circuit, and mobile application. The device enabled real-time monitoring of the changes in glucose and H_2O_2 concentrations, which could potentially provide a quantitative diagnostic aid for the diagnosis and treatment of diabetes. The microarrow structure was beneficial for the

sensor to anchor to the penetrated tissue, which could potentially enhance the sensor stability during sensing. The MASA was sensitive to real-time changes in glucose and H_2O_2 concentrations and exhibited a good linear response, excellent selectivity, temporal stability, reproducibility, and reliable signal transmission performance. The in vivo experimental results showed that the MASA was capable of monitoring glucose and H_2O_2 concentrations in real time with satisfying accuracy, where the detected H_2O_2 signal could be further utilized for assessing the inflammation issue during sensing. This work provided a promising strategy that would find widespread application for glucose level detection in subcutaneous tissue fluids, possessing potential clinical applicability and beneficial in aiding the diagnosis and treatment of diabetes as well as the monitoring of other biomarkers related to other diseases.

Supplementary Information The online version contains supplementary material available at https://doi.org/10.1007/s42242-023-00246-2.

Acknowledgements This work was financially supported by the National Key R&D Program of China (Nos. 2021YFF1200700 and 2021YFA0911100), the National Natural Science Foundation of China (Nos. 32171399, 32171456, and T2225010), the Guangdong Basic and Applied Basic Research Foundation (No. 2021A1515012261), the Science and Technology Program of Guangzhou, China (No. 202103000076), the Fundamental Research Funds for the Central Universities, Sun Yat-Sen University (No. 22dfx02), and Pazhou Lab, Guangzhou (No. PZL2021KF0003). The authors would also like to thank the Opening Project of Key Laboratory of Microelectronic Devices & Integrated Technology, Institute of Microelectronics, Chinese Academy of Sciences, and the Tianjin Key Laboratory of Imaging and Sensing Microelectronic Technology. FML would like to thank the National Natural Science Foundation of China (Nos. 32171335 and 31900954). JL would like to thank the National Natural Science Foundation of China (No. 62105380) and the China Postdoctoral Science Foundation (No. 2021M693686). QQOY would like to thank the China Postdoctoral Science Foundation (No. 2022M713645).

Author contributions XSH, BML, and XX conceived the concept, designed the work, and wrote the manuscript. XSH, MYH, STZ, BML, FFW, and JBY performed the experiments and statistical analyses. XSH, STZ, BML, HJC, and XX performed statistical analyses of datasets. QQOY, FML, and JL aided in the preparation of displays communicating datasets. HJC and XX supervised the study. All authors discussed the experimental results and assisted in the preparation and revision of the manuscript.

Declarations

Conflict of interest XX is an associate editor for *Bio-Design and Manufacturing* and was not involved in the editorial review or the decision to publish this article. We declare that we have no financial or personal relationships with other people or organizations that can inappropriately influence our work.

Ethical approval All animal procedures conducted in this work were reviewed, approved, and supervised by the Institutional Animal Care and Use Committee (IACUC) at Sun Yat-Sen University (approval numbers: SYSU-IACUC-2021-000022 and SYSU-IACUC-2021-000020).

References

1. Barrett-Connor E, Wingard D, Wong N et al (2018) Heart disease and diabetes. In: Diabetes in America, Bethesda
2. Rosenquist KJ, Fox CS (2018) Mortality trends in type 2 diabetes. In: Diabetes in America, Bethesda
3. Kitzmiller JL, Ferrara A, Peng T et al (2018) Preexisting diabetes and pregnancy. In: Diabetes in America, Bethesda
4. Yeh HC, Golozar A, Brancati FL (2018) Cancer and diabetes. In: Diabetes in America, Bethesda
5. Selvin E, Narayan KMV, Huang ES (2018) Quality of care in people with diabetes. In: Diabetes in America, Bethesda
6. Genuth SM, Palmer JP, Nathan DM (2018) Classification and diagnosis of diabetes. In: Diabetes in America, Bethesda
7. Teymourian H, Barfidokht A, Wang J (2020) Electrochemical glucose sensors in diabetes management: an updated review (2010–2020). Chem Soc Rev 49(21):7671–7709. https://doi.org/10.1039/d0cs00304b
8. Lee K, Goudie MJ, Tebon P et al (2020) Non-transdermal microneedles for advanced drug delivery. Adv Drug Deliv Rev 165–166:41–59. https://doi.org/10.1016/j.addr.2019.11.010
9. Schwartz AV, Lane NE (2018) Bone and joint complications in diabetes. In: Diabetes in America, Bethesda
10. Reutrakul S, Punjabi NM, van Cauter E (2018) Impact of sleep and circadian disturbances on glucose metabolism and type 2 diabetes. In: Diabetes in America, Bethesda
11. Metzger BE, Buchanan TA (2018) Gestational diabetes. In: Diabetes in America, Bethesda
12. Luchsinger JA, Ryan C, Launer LJ (2018) Diabetes and cognitive impairmen. In: Diabetes in America, Bethesda
13. Sanchez P, Ghosh-Dastidar S, Tweden KS et al (2019) Real-world data from the first US commercial users of an implantable continuous glucose sensor. Diabetes Technol Ther 21(12):677–681
14. Sharma S, Saeed A, Johnson C et al (2017) Rapid, low cost prototyping of transdermal devices for personal healthcare monitoring. Sens Biosens Res 13:104–108. https://doi.org/10.1016/j.sbsr.2016.10.004
15. Skyler JS, Krischer JP, Becker DJ et al (2018) Prevention of type 1 diabetes. In: Diabetes in America, Bethesda
16. Jina A, Tierney MJ, Tamada JA et al (2014) Design, development, and evaluation of a novel microneedle array-based continuous glucose monitor. J Diabetes Sci Technol 8(3):483–487. https://doi.org/10.1177/1932296814526191
17. Strambini LM, Longo A, Scarano S et al (2015) Self-powered microneedle-based biosensors for pain-free high-accuracy measurement of glycaemia in interstitial fluid. Biosens Bioelectron 66:162–168. https://doi.org/10.1016/j.bios.2014.11.010
18. Gao W, Emaminejad S, Nyein HYY et al (2016) Fully integrated wearable sensor arrays for multiplexed in situ perspiration analysis. Nature 529(7587):509–514. https://doi.org/10.1038/nature16521
19. Mohan AMV, Windmiller JR, Mishra RK et al (2017) Continuous minimally-invasive alcohol monitoring using microneedle sensor arrays. Biosens Bioelectron 91:574–579. https://doi.org/10.1016/j.bios.2017.01.016
20. Wang C, Li X, Hu H et al (2018) Monitoring of the central blood pressure waveform via a conformal ultrasonic device. Nat Biomed Eng 2(9):687–695. https://doi.org/10.1038/s41551-018-0287-x
21. Takeuchi K, Takama N, Kim B et al (2019) Microfluidic chip to interface porous microneedles for ISF collection. Biomed Microdev 21:28. https://doi.org/10.1007/s10544-019-0370-4
22. Liu F, Lin Z, Jin Q et al (2019) Protection of nanostructures-integrated microneedle biosensor using dissolvable polymer coating. ACS Appl Mater Interfaces 11(5):4809–4819. https://doi.org/10.1021/acsami.8b18981

23. Nelson BB, Stewart RC, Kawcak CE et al (2021) Quantitative evaluation of equine articular cartilage using cationic contrast-enhanced computed tomography. Cartilage 12(2):211–221. https://doi.org/10.1177/1947603518812562
24. Xiao Z, Zhou W, Zhang N et al (2019) All-carbon pressure sensors with high performance and excellent chemical resistance. Small 15(13):e1804779. https://doi.org/10.1002/smll.201804779
25. Teymourian H, Tehrani F, Mahato K et al (2021) Lab under the skin: microneedle based wearable devices. Adv Healthc Mater 10(17):e2002255. https://doi.org/10.1002/adhm.202002255
26. Jiang X, Lillehoj PB (2020) Microneedle-based skin patch for blood-free rapid diagnostic testing. Microsyst Nanoeng 6:96. https://doi.org/10.1038/s41378-020-00206-1
27. Goud KY, Moonla C, Mishra RK et al (2019) Wearable electrochemical microneedle sensor for continuous monitoring of levodopa: toward Parkinson management. ACS Sens 4(8):2196–2204. https://doi.org/10.1021/acssensors.9b01127
28. Invernale MA, Tang BC, York RL et al (2014) Microneedle electrodes toward an amperometric glucose-sensing smart patch. Adv Healthc Mater 3(3):338–342. https://doi.org/10.1002/adhm.201300142
29. Ribet F, Stemme G, Roxhed N (2018) Real-time intradermal continuous glucose monitoring using a minimally invasive microneedle-based system. Biomed Microdevices 20(4):101. https://doi.org/10.1007/s10544-018-0349-6
30. Klawitter JJ, Patton J, More R et al (2020) In vitro comparison of wear characteristics of pyrocarbon and metal on bone: shoulder hemiarthroplasty. Shoulder Elbow 12(1 Suppl):11–22. https://doi.org/10.1177/1758573218796837
31. Samavat S, Lloyd J, O'Dea L et al (2018) Uniform sensing layer of immiscible enzyme-mediator compounds developed via a spray aerosol mixing technique towards low cost minimally invasive microneedle continuous glucose monitoring devices. Biosens Bioelectron 118:224–230. https://doi.org/10.1016/j.bios.2018.07.054
32. Li CG, Joung HA, Noh H et al (2015) One-touch-activated blood multidiagnostic system using a minimally invasive hollow microneedle integrated with a paper-based sensor. Lab Chip 15(16):3286–3292. https://doi.org/10.1039/c5lc00669d
33. Keum DH, Jung HS, Wang T et al (2015) Microneedle biosensor for real-time electrical detection of nitric oxide for in situ cancer diagnosis during endomicroscopy. Adv Healthc Mater 4(8):1153–1158. https://doi.org/10.1002/adhm.201500012
34. Li X, Huang X, Mo J et al (2021) A fully integrated closed-loop system based on mesoporous microneedles-iontophoresis for diabetes treatment. Adv Sci 8(16):e2100827. https://doi.org/10.1002/advs.202100827
35. Pang Q, Lou D, Li S et al (2020) Smart flexible electronics-integrated wound dressing for real-time monitoring and on-demand treatment of infected wounds. Adv Sci 7(6):1902673. https://doi.org/10.1002/advs.201902673
36. Samant PP, Niedzwiecki MM, Raviele N et al (2020) Sampling interstitial fluid from human skin using a microneedle patch. Sci Trans Med 12:eaaw0285. https://doi.org/10.1126/scitranslmed.aaw0285
37. Chinnadayyala SR, Park I, Cho S (2018) Nonenzymatic determination of glucose at near neutral pH values based on the use of nafion and platinum black coated microneedle electrode array. Mikrochim Acta 185(5):250. https://doi.org/10.1007/s00604-018-2770-1
38. Miller P, Moorman M, Manginell R et al (2016) Towards an integrated microneedle total analysis chip for protein detection. Electroanalysis 28(6):1305–1310. https://doi.org/10.1002/elan.201600063
39. Dervisevic M, Alba M, Yan L et al (2021) Transdermal electrochemical monitoring of glucose via high-density silicon microneedle array patch. Adv Funct Mater 32(3):2009850. https://doi.org/10.1002/adfm.202009850
40. Parrilla M, Cuartero M, Sanchez SP et al (2019) Wearable all-solid-state potentiometric microneedle patch for intradermal potassium detection. Anal Chem 91(2):1578–1586. https://doi.org/10.1021/acs.analchem.8b04877
41. Yang SY, O'Cearbhaill ED, Sisk GC et al (2014) A bio-inspired swellable microneedle adhesive for mechanical interlocking with tissue. Nat Commun 4:1702. https://doi.org/10.1038/ncomms2715
42. Han D, Morde RS, Mariani S et al (2020) 4D printing of a bioinspired microneedle array with backward-facing barbs for enhanced tissue adhesion. Adv Funct Mater 30(11):1909197. https://doi.org/10.1002/adfm.201909197
43. Jin Q, Chen HJ, Li X et al (2019) Reduced graphene oxide nanohybrid-assembled microneedles as mini-invasive electrodes for real-time transdermal biosensing. Small 15(6):1804298. https://doi.org/10.1002/smll.201804298